XLI CILAMCE
XLI Ibero-Latin American Congress on Computational Methods in Engineering
16-19 November, 2020 FOZ DO IGUAÇU PARANÁ - BRAZIL

Numerical analysis of the influence of welding speed on cylindrical pressure vessels

Fernanda F. Santos[1]

[1]*Dept. of Materials, University of Sergipe*
Avenue Marechal Rondon,49100-000, Sergipe, Brazil
ffernaand@gmail.com

Abstract. This work aims to determine the residual stresses of cylindrical pressure vessels subjected to weld repairs via numerical analysis . In welding repair , a glove is attached to the pressure vessel through two longitudinal welds and two circumferential welds . Was performa modeling of the pressure vessels , the repair and the welds acoording to the standart . The parameters of the weld bead will be adopted on the basis of what happens in practice , and this will be done the analyzes of the residual stresses varying the speed of the weld bead . From this , will be analyzes the residual stresses in the regions of the weld to verify the behavior of the results after the cooling period by the Finite Element Method .

Keywords: Finit element method 1. Pressure vessel 2. Welding 3.

1 Introduction

Pressure vessels are present and important equipment in many chemical and petrochemical industries, sugar and ethanol plants, pharmaceuticals, among others, and are also widely used for industrial processes involving fluids or gases, which operate with internal pressures other than atmospheric pressure. Or according to the NR-13 of 2014, pressure vessels are equipment that contain fluids under internal or external pressure, different from atmospheric pressure. The vast majority of pressure vessels are manufactured from the union of steel sheets using the welding process. However, this process causes distortions in the base material. These distortions can cause the equipment to fail. Because of this, it is important to take the utmost caution during the process of choosing the weld bead parameters, as well as the procedures established in the standards for its repair or manufacture must be followed, as this way the necessary steps are guaranteed to maintain the structural integrity pressure vessel and do not damage the environment involved.

Engineers carry out studies on the assessment of structural integrity in various situations, such as repairing, designing or even assessing whether the equipment complies with the standards and is widely used in maintenance stops to assess whether or not the equipment can continue in operation . These assessments can be performed by several softwares, such as: ANSYS, COSMOS / M, NASTRAN, ABAQUS, among others, which use numerical analysis based on the finite element method (MEF). The present work aims to obtain results, using the finite element method, such as residual stresses and total heat flow, by conducting thermal and structural transient analyzes to determine the residual stresses in the pressure vessel caused by the variation in the velocity of welding in the pressure vessel.

2 Modeling

The pressure vessel in question is used in a petrochemical industry, which shows a loss of thickness caused by corrosion, used as an activated carbon filter as shown in Figure (1). For reasons of technical design and construction requirements, this vessel is made of ASTM A516 Grade 70 steel (austenitic stainless steel of the low carbon non- sensitive type). This material is widely used for the construction of pressure vessels, as it has a good capacity to absorb energy when a failure is present and high resistance to corrosion.

Figure 1 - Photograph of the studied activated carbon filter.

The following working characteristics of the pressure vessel are: working pressure of 2.07 MPa; working temperature of 177oC; internal diameter of 1.22 m; thickness: 19.05 mm; permissible stress of 137.70 MPa. The step by step of the geometric model of the pressure vessel-repair-weld assembly is described in (Almeida, 2017). Figure (2) shows the result of the modeling.

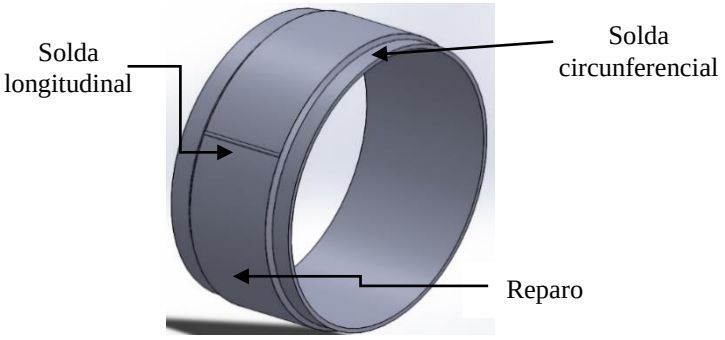

Figure 2 – Modelagem completa do conjunto vaso de pressão-reparo-solda.

Figure (3) shows the mechanical properties of the pressure vessel assembly .

ASTM A516 Gr. 70	Propriedades	
Densidade (Kg/m³)	7960	
Condutividade térmica (W/m.K)	58	
Calor específico (J/kg.K)	521	
Coeficiente de expansão térmica (1/ºC)	100ºC	1,31e-6
	200ºC	1,37e-6
	300ºC	1,41e-6
	400ºC	1,43e-6
	450º	1,44e-6
Módulo de Young (10^3 MPa)	20ºC	206,8
	300ºC	201,3
	400ºC	196,7
	450ºC	194,3
Limite de escoamento(MPa)	20ºC	262
	300ºC	234
	400ºC	230
	450ºC	226
Módulo tangente (MPa)	431,4	
Resistência última a tração (MPa)	482,6	
Coeficiente de Poisson	0,303	

Table 1 - Mechanical Properties for ASTM A516 Grade 70 steel.

The plasticity model adopted was elastoplastic with linear hardening and the melting temperature of the material is 1873 ° C. The material stress x strain diagram can be found in Almeida, 2017.

2.1 Mesh generation

In the case of this work, an input parameter of 7 mm will be used as the size of the element for generating the mesh. This value was selected by adopting at random, but so that this value was less than the shortest distance in the pressure vessel set, which in this case is 15.70 mm, corresponding to the upper surface of the longitudinal weld, as shown in Figure (4) , so that they have results of the analyzes in that region.

A lower value of the element size mentioned above could generate problems during the convergence of the results, in addition to generating a larger amount of data to be processed, requiring better computers for processing.

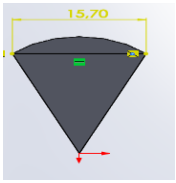

Figure 4 - Width of the longitudinal weld bead.

Based on these data, a total of 46,898 elements and 124,206 nodes were generated. The mesh was also composed of 10-node tetrahedral elements and 20-node hexahedral elements. This choice of composition is made by the program itself, based on the complexity of the geometry.

2.1.1 Boundary conditions for thermal transient analysis

In the thermal transient analysis, convection and radiation from the environment will be used as boundary conditions for the numerical solution. Figure (5) shows the external surfaces of the pressure and repair vessel, and the external surfaces of the longitudinal and circumferential welds on which the convection conditions determined below, imposed by the so-called Newton's Cooling Law given by Equation (1), will be imposed.:

$$Q = Ah (Ts - T \bowtie) \quad (1)$$

On what:
Q - Heat transfer rate [W / mm²];
h - Convective coefficient;
Ts - Surface temperature [ºC];
A - Heat transfer area;

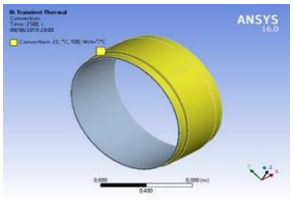

Figure 5 - Condition of convection by the environment on the surfaces.

According to INCROPERA, et al., (2008):
h = 0.0005 W / m ^ 2 ºC
(T) _ ⋈ = 22 ° C
Similarly, the radiation boundary condition is applied to the external surfaces of the pressure vessel and the repair, as shown in Figure (6).

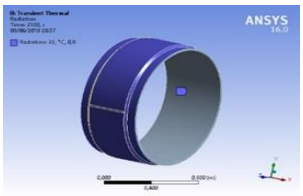

Figure 6 - Condition of radiation contour by the environment on the surfaces .

According to INCROPERA, et al., (2008) and the so-called Stefan Boltzann Law given by Equation (2), we have:

$$Q = \varepsilon\sigma (Ts \text{ ^ } 4\text{-}Tviz \text{ ^ } 4) \quad (2)$$

On what:
ε - Emissivity - ε = 0.8
σ - Stefan-Boltzmann constant = 5.67x10-8 W / (m².K ^ 4).
Ts - Surface temperature [oC];
Tviz - Room temperature;
Finally, for this analysis, it is necessary to establish some input data, such as weld bead speed and heat source intensity, which will be described below.

2.1.2 Weld bead speed

In this work, the width of the chamfer V is 15.70 mm (Almeida, 2017). Based on this information and according to FANOUS, YOUNAN, et al. (2011) the electrode radius was chosen as 25 mm, since the thermally affected zone reaches the repair beyond the formed chamfer.

For each chosen speed, it will be necessary to determine the start time and end time for two longitudinal and circumferential welds. For the first longitudinal weld, taking the weld speed of 6 mm / s and the weld length of 368.3 mm, same length as the repair, it is possible to calculate using Equation (3):

A preparation time for the next weld of 20 s is given for each welding end. The first longitudinal weld was also given a time interval of 20 s before the start of welding. Table (1) shows the time to first weld.

Table 1 - Time input data for the third thermal load.

Initial weld time	182,76 seconds
Final weld time	841,08 seonds

Analogously, the same is done for the second circumferential weld, always using the preparation time of the weld and the same welding feeling as the first circumferential weld. Tab. (2) shows the times for the second circumferential weld:

Table 2 - Time input data for the fourth thermal load.

Initial weld time	861,08 seconds
Final weld time	1519,4 seconds

A cooling time is considered at the end of the welding process of the pressure-repair vessel, so 2200 s will be used instead of 1519.4 s.

Similarly, the same is done to calculate the welding times for speeds of 7 mm / s and 8 mm / s, shown in Table (3), in order to better observe the behavior of the welding speed variation.

Speed 7 mm/s	
Longitudinal welding time	52,61 s
Longitudinal welding time 1	
Initial	20 s
Final	72,61 s
Longitudinal welding time 2	
Initial	92,61 s
Final	145,22 s
Circumferential weld time	658,31 s
Circumferential welding time 1	
Initial	165,22 s
Final	729,50 s
Circumferential welding time 2	
Initial	749,50 s
Final	1313,77 s
End time with cooling	2000 s

Speed 8mm/s	
Longitudinal welding time	46,04 s
Longitudinal welding time 1	
Initial	20 s
Final	66,04 s
Longitudinal welding time 2	
Initial	86,04 s
Final	132,07 s
Circumferential weld time	493,73 s
Circumferential welding time 1	
Initial	152,07 s
Final	645,81 s
Circumferential welding time 2	
Initial	665,81 s
Final	1159,55 s
End time with cooling	1800 s

Table 3 - Time input data for thermal load for speeds a) 7 mm/s e b) 8 mm/s

All of this weld bead time data was inserted into an extension of ANSYS 16.0, called Moving Heat Flux, which simulates the passage of a weld bead in a material.

2.1.3 Solder source intensity

In the last stage, there is the essential thermal load necessary for the intensity of the heat source. This thermal load depends on three factors: electrical current, voltage and efficiency of the weld. These parameters were selected based on FANOUS, YOUNAN, et al., (2003), with this, an intensity of 15.3 W / mm2 was found. As the speed adopted in this work is less than 1 m / min, according to Schwedersky et al., 2011, it is not necessary to increase the welding current.

2.1.4 Boundary conditions for structural transient analysis

For the structural transient analysis, the boundary restriction (bonded) at both ends of the pressure vessel that prevents movement in the six degrees of freedom will be used as the boundary condition

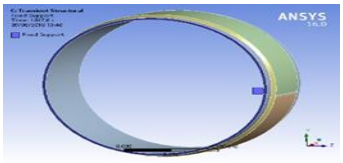

Figure 7 - Condition of boundary boundary contour at the ends of the pressure vessel.

3 Results

Figure (8) shows the temperature distribution as a function of time during the welding process according to each speed, as shown in the graph legend.

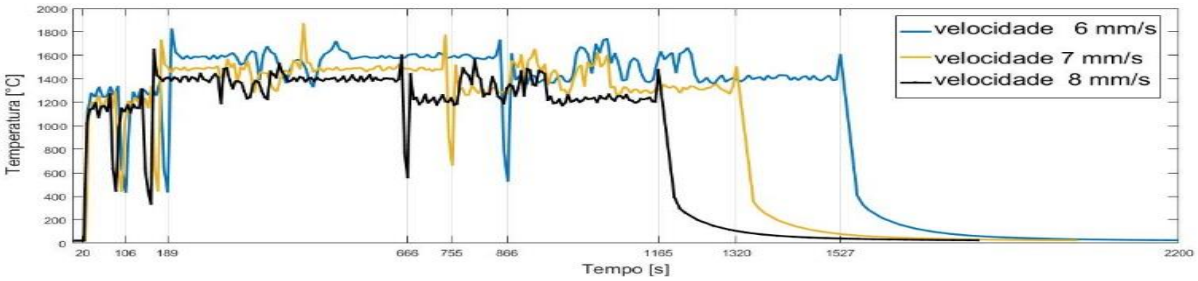

Figure 8 - Temperature distributions as a function of time.

It is noted through the graph that even with the difference in speed, consequently in time, there is a standard behavior followed by the three curves represented, with the existence of the temperature difference resulting from the change in speed, which decreases with increasing speed. Therefore, this feature allows us to divide the graph into five regions for all speeds, which can be described as follows:

• First region: comprises the interval from 0 to 20 seconds, which can be described as preparation time for welding keeping the ambient temperature around 22 ° C. In addition to the start of the first longitudinal weld, a rapid increase in temperature (first temperature peak) is noticed.

• Second region: this region is similar to the first region, characterized by the beginning of the second longitudinal weld, in which there is a decrease in temperature, cooling, referring to the 20 seconds of preparation of the weld and then the second longitudinal weld is started, presenting the second temperature peak on the graph.

• Third region: this region corresponds to the first circumferential weld, starting with the preparation of the weld, corresponding to 20 seconds. In the graph, this beginning is represented by the second cooling region. Then the process of the first circumferential weld starts, in which it is possible to observe the third peak of temperature due to the beginning of heating, added to the heat already absorbed in the longitudinal welds carried out. In addition to having a longer time region than the previous ones, due to the greater path taken during the welding process.

• Fourth region: this region corresponds to the second circumferential weld, similar to the third region. Started with the 20 seconds of preparation of the weld, being represented by the third cooling region. Soon after, the fourth temperature peak is presented, a consequence of the beginning of the welding process, presenting characteristics described in the third region.

• Fifth region: it is the cooling region for all speeds, characterized by a temperature decay, presenting a final temperature close to the environment, 22 ° C, due to convection and radiation.

Figure (9) presents the data of the total heat flow distribution resulting from the thermal transient analysis, according to each speed.

Comparing Figure (8) to the previous graph of the temperature distribution in the pressure vessel assembly, it is possible to notice a similar behavior due to the proportionality between heat flow and temperature. Because of this same proportionality, it can be explained in relation to the graph curves, the increase in the heat flow with the decrease in speed.

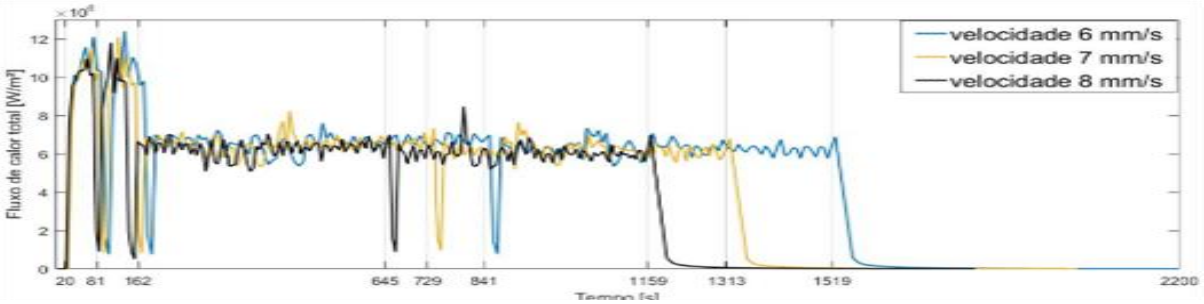

Figure 9 - Total heat flow distributions as a function of time.

Given by Equation (3), the heat flow through a surface is provided by the relationship between the amount of heat Q that passes through the surface and the elapsed time interval.

$$\Phi = Q / \Delta t \tag{3}$$

The value of Q can be calculated by the equations below, emphasizing that the predominance for welding is the heat flow are convection and conduction, respectively.

$$Q = h (T_s - T_{\bowtie}) \quad (4)$$

$$Q = - k (dT / dx) \quad (5)$$

Observing the region of total heat flow with higher peaks, Figure (9), we find, for all speeds, the regions of the longitudinal welds differently from what can be observed in the temperature distribution, as there is a change in geometry and chamfer in welding, which affects the convection coefficient, since it is influenced by geometry, flow regime and the type of fluid.

Figure (10a), Figure (10b) and Fig (10c) show the von Mises stresses in the structure for speeds 6 mm / s, 7 mm / s and 8 mm / s, respectively.

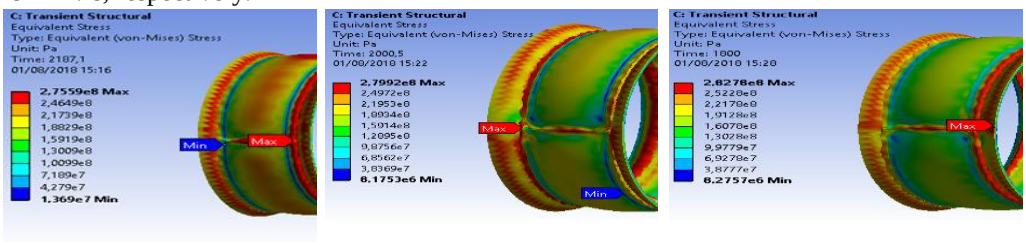

a) b) c)

Figure 10 - Distribution of von Mises stresses in the structure for speed a)6 mm / s b) 7mm/s e c) 8 mm/s

It is possible to conclude through Figures (10a), (10b) and (10c) that the greatest von Mises stresses observed occur in the central region and in the vicinity of the longitudinal and circumferential welds, observed by the red regions. Comparing the three figures, it is also verified that there is an increase in von Mises tension accompanied by an increase in speed.

Still analyzing the previous thermal images, Figure (10a), (10b) and (10c), with Figure (11) it is also possible to affirm, by the formation of the region in red color, that the most critical area observed in relation to longitudinal welds , is the first longitudinal weld for all speeds, also caused by the sum of the thermal effects caused by the subsequent welds and cooling time.

In Figure (11) it is possible to notice a proportionality in relation to Figure (8). In the distribution of the plastic deformation, it is possible to notice that the first two well-defined regions, referring to the two longitudinal welds, appear in a shorter period of the graph compared to the other areas and have lower values due to the shorter welded path. The next region is shown to have much higher values due to the longer path, consequently greater time and greater plastic deformations will be obtained during the welding process in these conditions. In relation to each curve, the decrease in plastic deformation with the increase in speed is noticeable, caused by the decrease in time according to the speed and thus decrease in the energy of the welding process at each point.

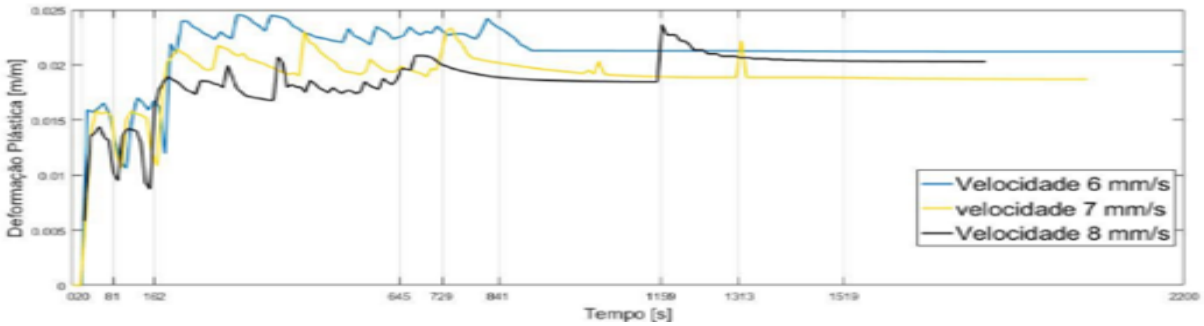

Figure 11 - Distribution of Plastic Deformation in the pressure vessel assembly.

4 Conclusions

According to the results obtained through the approached method, it can be seen that despite the small variation, only 1mm / s of the welding speed, significant results were obtained in the fields of von Mises stresses , temperature, total heat flow and plastic deformations, in addition to making it possible to discuss the behavior and causes of the results obtained for each welding speed, in which a series of factors must be considered, such as geometry and time. Also providing results that allow the study with other welding parameters to obtain the ideal point of the process.

References

[1] Almeida, J.I.L., 2017, "Determinação das tensões residuais via análise numérica transiente térmica de vasos de pressão submetidos a reparos por soldagem", Tese – Universidade Federal da Paraíba.
[2] Baker, A.J., 2012, "Finite Elements: Computational Engineering Sciences", 1o Edition, John Wiley & Sons, Ltd, USA.
[3] Chandrupatla, T.R., belegundu, A.D., "Elementos finitos", editora Person, 4ª ed., 2014.
[4] Harvey, J.F.,"Theory and Design of Modern Pressure Vessels", Van Nostrand Reinhold Co, New York, 1974.
[5] Incropera [et al.]., "Fundamentos de transferência de calor e de massa", 6ª Edição LTC, Rio de Janeiro.
[6] Paiva, V.E.L., "Simulação de tensões residuais de soldagem e seu alívio por teste hidrostático", dissertação de metrado, Puc-Rio, 2015.
[7] Savage, W. F.; nippes, E. F.; Agusa, K. "Effect of Arc Force on Defect Formation in GTA Welding" Welding Journal, jul. 1979. 212s-224s.
[8] Schwedersky, M.B., Dutra, J.C., Okuyama, M.P., Silva, R.H.G., "High Productivity TIG Welding: Influence of Shielding Gases on the Limit Speed for Defect Formation", Santa Catarina, Brasil, 2011.